eprints@whiterose.ac.uk
https://eprints.whiterose.ac.uk/

Self-Assembled InAs Quantum Dots on InGaAsP/InP(100) by Modified Droplet Epitaxy in Metal–Organic Vapor Phase Epitaxy around the Telecom C-Band for Quantum Photonic Applications

Elisa M. Sala,* Young In Na, Max Godsland, and Jon Heffernan

The growth of InAs quantum dots (QDs) by droplet epitaxy (DE) in metal–organic vapor phase epitaxy is demonstrated for the first time on an InGaAsP layer lattice matched to InP(100). The nucleation of indium droplets on InGaAsP shows a strong dependence on the deposition temperature, with an unexpectedly low density, pointing to a strongly increased surface diffusion compared to bare InP or InGaAs surfaces previously reported. Droplets and surface morphology are characterized via atomic force microscopy and scanning electron microscopy. Droplet crystallization into InAs QDs is explored, where the crystallization process follows a modified DE growth which resembles the one on InGaAs but strongly differs from bare InP. Also, no formation of quantum dashes (QDashes) is observed, as the DE growth technique used here allows for a better control of QD nucleation, decoupled from the layer/epilayer mismatch, favoring the formation of QDs over QDashes. Optical characterizations suggest a more efficient carrier capture into the QDs if these are grown on InGaAsP compared to InGaAs. Finally, bright single-dot emission at low-temperature is detected from QDs ranging from 1300 to 1600 nm, covering the technologically relevant telecom C-band.

1. Introduction

III-V self-assembled semiconductor quantum dots (QDs) have been the subject of extensive studies over the last few decades, owing to their unique physical properties.[1,2] They find applications as the active medium in lasers,[3–5] as sources of pure single photons and entangled photon pairs for quantum information technologies,[6] and as building blocks for novel nanomemory devices.[7–9] In particular, InAs/InP QDs are currently very attractive as single-photon emitters due to their compatibility with the low-loss telecom C-band at 1.55 μm.[10,11] Droplet epitaxy (DE) in metal–organic vapor phase epitaxy (MOVPE) is a recent and very promising approach for QD fabrication, as it combines a large-scale epitaxial technique and a versatile epitaxial method.[12–15] This is a relatively new process that is not fully understood in terms of growth dynamics, particularly for III-V material systems compatible with telecom wavelengths, such as InAs/InP. Thus, it holds great potential for further development in the fabrication of telecom QDs for a broad range of applications. Additionally, using InP as matrix material allows for the growth of InAs quantum emitters without the assistance of any additional metamorphic buffer, such as AlInAs/GaAs.[16–18] InAs/InP QDs grown by DE in MOVPE show high symmetry[12,15,19] and consequently lower FSS and longer coherence times compared to their Stranski–Krastanow (SK) counterparts.[18,20] They are thus excellent candidates as high-quality photon sources for photonic devices. Compared to the standard SK mode for QD growth, DE is a much more versatile method allowing for the fabrication of QDs and nanostructures with a wider range of material combinations as it does not rely on lattice-mismatch for nanostructure formation, but on crystallization of group III metallic droplets.[21] Previously, we studied InAs DE QDs on both bare InP[12,13] and on an $In_{0.53}Ga_{0.47}As$ surface lattice matched to InP.[14] The latter showed QD nucleation following a modified DE mode compared to growth on InP, without the formation of etch pits around the QDs and generally higher QD density of 10^8–10^{10} cm^{-2} were achieved. The major change to the DE growth was associated with crystallization on an As-terminated surface, versus the P-terminated surface of InP. In this article, we continue the investigation of growth dynamics on a new surface type and study the DE of InAs QDs on a quaternary InGaAsP layer lattice-matched to InP where there is a mixed As/P termination. To the best of our knowledge, this

E. M. Sala
EPSRC National Epitaxy Facility and Department of Electronic and Electrical Engineering
The University of Sheffield North Campus
Broad Lane, S37HQ Sheffield, UK
E-mail: e.m.sala@sheffield.ac.uk

Y. I. Na, M. Godsland
Department of Electronic and Electrical Engineering
The University of Sheffield North Campus
Broad Lane, S37HQ Sheffield, UK

J. Heffernan
EPSRC National Epitaxy Facility and Department of Electronic and Electrical Engineering
The University of Sheffield North Campus
Broad Lane, S37HQ Sheffield, UK

The ORCID identification number(s) for the author(s) of this article can be found under https://doi.org/10.1002/pssr.202300340.

DOI: 10.1002/pssr.202300340

is the first report of telecom InAs QDs embedded in InGaAsP/InP grown by DE in an MOVPE environment. We first study indium droplet formation for a wide range of deposition temperatures and compare the results with our previous findings on InP and InGaAs surfaces. Next, their crystallization into QDs is studied. QDs densities ranging from 8×10^8 to 2×10^{10} cm^{-2} are achieved and the QDs show bright single-dot emission at low-temperature in the range 1300–1600 nm. These QDs are suitable for various device applications between telecom O-, C-, and L-bands, such as single-photon sources, as well as an active medium for lasers as, unlike the SK QDs, they do not present a wetting layer. In this context, the investigation of InAs QD growth embedded in InGaAsP/InP is particularly important given the extensive use of this quaternary alloy as waveguide material for telecom lasers.[22–24]

2. Results and Discussion

We studied the formation of indium droplets on a 5 nm InGaAsP interlayer, with varying deposition temperature ranging from 250 to 400 °C. AFM micrographs are shown in **Figure 1**. Figure 1a,b shows that macroscopic In droplets can be clearly detected only at 400 and 350 °C, respectively, while for lower temperatures no droplets can be observed. At 320 °C, Figure 1c, the surface morphology appears relatively rough with an RMS roughness of 230 pm, whilst for the lowest temperatures of 280 and 250 °C, Figure 1d,e, ML-steps typical of step-flow growth can be seen with a RMS roughness of 155 and 145 pm, respectively, and consistent with good quality layer-by-layer InP growth.[25] At 320 °C, the surface transitions to In clustering, resulting in the altered surface roughness (230 pm), but without yet showing macroscopic In droplets.

The absence of droplets or In wetting below 320 °C is due to the fact that the TMIn precursor for In is not pyrolyzed.[26–28] When the temperature is further increased to 350 °C, the first macroscopic droplets nucleate on the InGaAsP surface (Figure 1b). The same sample surfaces but with larger areas are displayed in **Figure 2**, where the images were taken by SEM. This allowed us to determine the droplet density at the temperatures of 350 and 400 °C more precisely. In particular, droplets have a density of 3×10^6 and 1×10^6 cm^{-2} at 350 and 400 °C, respectively. The diameters of the droplets are of $\approx$425 and $\approx$750 nm at 350 and 400 °C, respectively. Droplet heights have been extrapolated from the AFM analysis and are $\approx$90 and $\approx$105 nm for 350 and 400 °C, respectively.

Previously, we studied indium droplet deposition on both bare InP and an In$_{0.53}$Ga$_{47}$As surface lattice matched to InP.[12,14] For InGaAs, we found that droplets had almost two orders of magnitude greater density compared to InP, together with an overall reduced size. We ascribed this to a lower In surface diffusion on InGaAs compared to InP.[14,29] In **Figure 3**, we summarize the droplet density for all three surfaces considered: InP,[12] InGaAs,[14] and InGaAsP (this study) at the same droplet deposition temperature of 400 °C. Unexpectedly, on InGaAsP, we find that droplets have an even lower density compared to InP (1×10^6 vs 6×10^7 cm^{-2}).

Figure 4 shows AFM micrographs of In droplets at 400 °C on the three different surfaces under consideration: (a) InGaAs, (b) InP, and (c) InGaAsP. Note the different image sizes used for a better visualization of the droplet densities. Compared to what one would expect, that is finding a droplet density lying in-between the ones of InP and InGaAs, droplets on InGaAsP are the largest with the lowest density: a striking $\approx$30 times wider and $\approx$10 times higher than those on InGaAs, while 10 times wider and twice as high as droplets on InP.
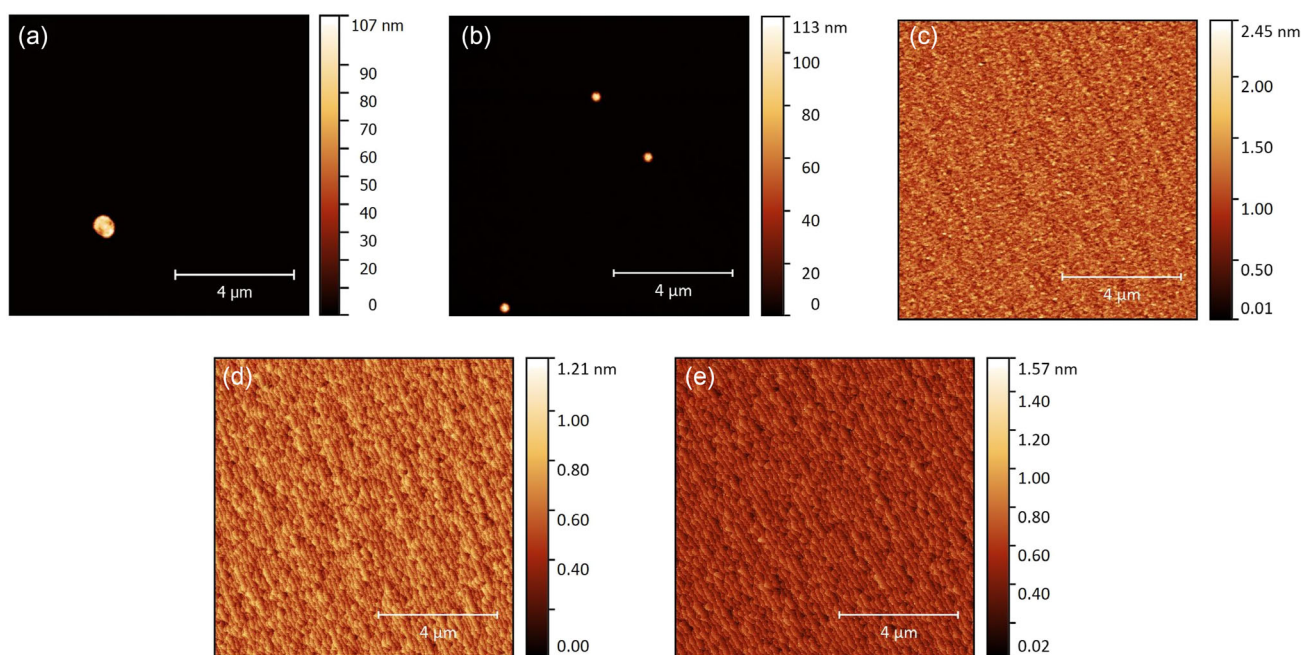
Figure 1. 10×10 µm^2 AFM micrographs of free-standing indium droplets on 5 nm InGaAsP/InP surfaces deposited at substrate temperatures of a) 400 °C, b) 350 °C, c) 320 °C, d) 280 °C, and e) 250 °C.
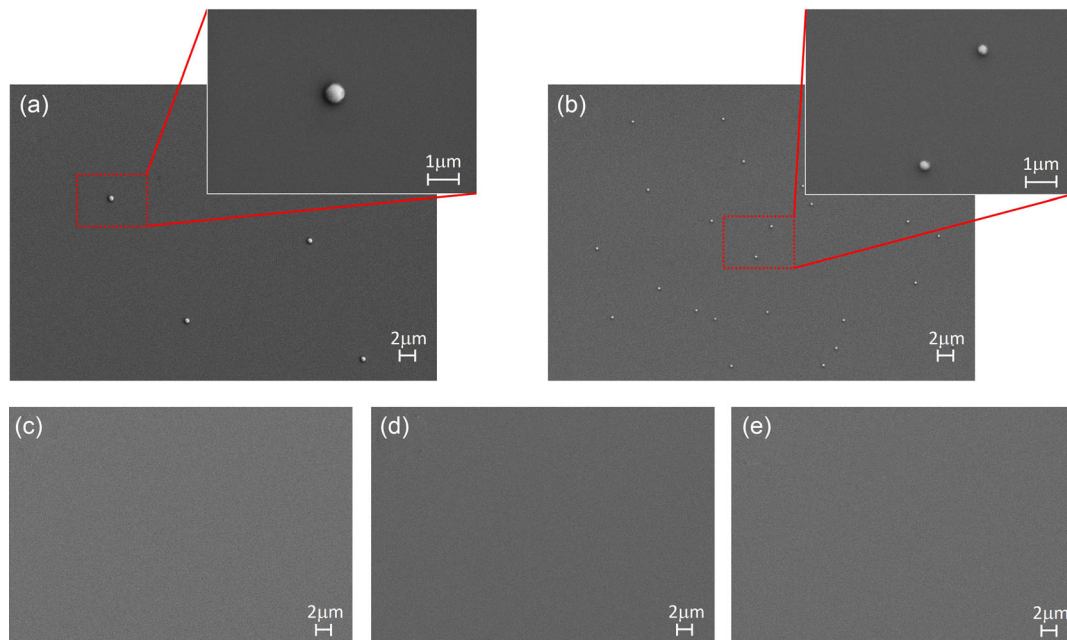
Figure 2. SEM micrographs of free-standing indium droplets on 5 nm InGaAsP/InP surfaces deposited at substrate temperatures of a) 400 °C, b) 350 °C, c) 320 °C, d) 280 °C, and e) 250 °C. Acceleration voltage of 10 kV and magnification of 5000 for a–e) and 30 000 for the magnified areas in the insets of (a) and (b).
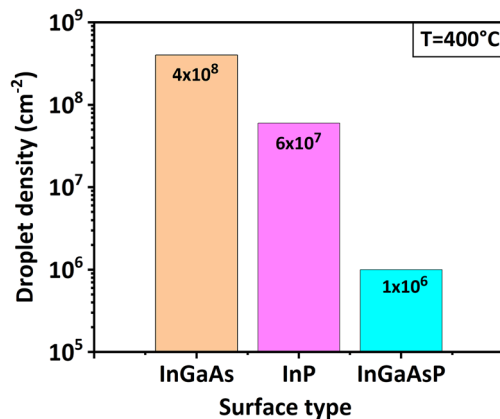
Figure 3. Indium droplet densities on the three different surfaces (InGaAs, InP, and InGaAsP) at the same deposition temperature of 400 °C.

We ascribe such considerable variation of droplet sizes and densities to a modification of the surface diffusion. From these observations, we can conclude that the InGaAsP surface presents the highest surface diffusion among the three surfaces, which leads to a very low droplet density with the largest size. This unexpectedly high surface diffusion for the InGaAsP surface can be explained in terms of its surface configuration. For the $In_xGa_{1-x}As_yP_{1-y}$/InP system, a phase separation at the surface during epitaxial growth exists, also referred to as lateral composition modulation (LCM).[30–33] Specifically, LaPierre et al.[30] found that a preferential sticking of P atoms to Ga sites and of As to In takes place, which results in the formation of GaP and InAs-rich areas. They also found that LCM is strongly dependent on the InGaAsP surface orientation and composition, being more pronounced for the (100) orientation and for 1.3 μm bandgap wavelength, which corresponds to the case investigated here. In fact, the (100) InGaAsP surface, compared to other orientations, presents the
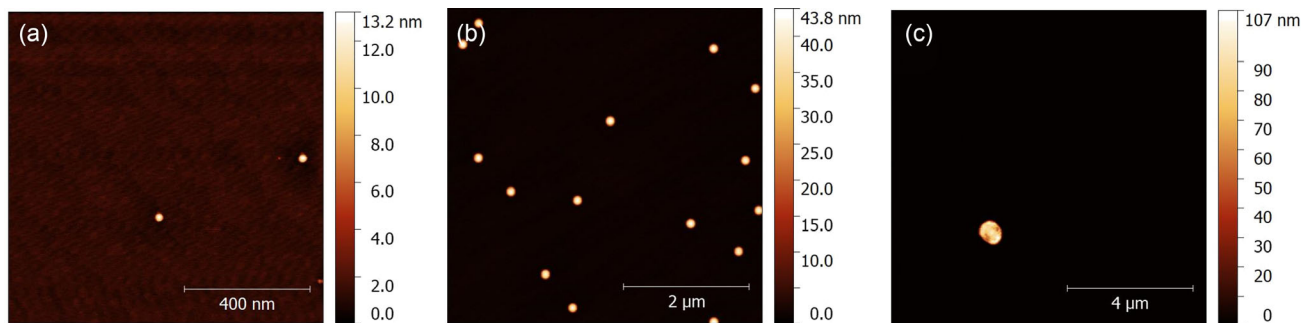

Figure 4. AFM micrographs of free-standing In droplets deposited at 400 °C on the three different surface types: a) InGaAs, b) InP, and c) InGaAsP. Note the different sizes of the scan areas adjusted for better visualization of the droplet densities.

highest number of group-III dangling bonds which are easily saturated by the impinging As and P, resulting in a greater LCM. Also, greater LCM appears to be correlated with an increased adatom surface diffusion, as this configuration will decrease the adatom incorporation rate.[30,34] Therefore, in our case, the diffusion of the In adatoms will be strongly enhanced by the InGaAsP LCM. This phenomenon can thus qualitatively explain the discrepancy of diffusion lengths observed for InGaAsP compared to InP and InGaAs.

Next, droplet crystallization into QDs is studied and compared to our previous results for droplet epitaxy InAs QDs on an InGaAs surface,[14] where the same droplet and crystallization conditions were used. As outlined in the Experimental Section, In droplets are exposed to an AsH_3 flow while the substrate temperature is increased to 520 °C for full droplet crystallization into QDs. **Figure 5** shows AFM micrographs of (a), (b) free-standing droplets and (c), (d) surface QDs, for the two surfaces considered. For both surface types QDs can be clearly detected. As a note, a direct comparison with the case of bare InP[12] is not given here, since for the droplet deposition temperature used here (400 °C) no QDs were observed. Here, we observe that crystallized InAs/InGaAsP QDs, Figure 5c, have a higher density than the initial droplets (Figure 5a). This is the same trend seen for InAs/InGaAs QDs, Figure 5b,d, as also previously reported by us.[14] Thus, we can confirm that there is a modified droplet crystallization into QDs in the case of InGaAsP as well as InGaAs. However, here we additionally note that the initial droplets are much bigger than the resulting QDs, which is not the case for the In droplets on InGaAs (Figure 5b). We attribute this to an out-diffusion of indium and

redistribution on the InGaAsP surface during the thermal ramp step which can lead to a reduction in droplet size and a "re-wetting" of the surface.[35] As for the case of QDs on InGaAs, no long-range etch pits around each QD are present.[12,13,15] From these observations, we can conclude that inserting the InGaAs(P) layers results in a modification of the growth kinetics from a mass-transport regime (on bare InP) to a surface reaction-limited regime on the interlayers, as previously suggested in our cross-sectional tunneling microscopy (XSTM) study on InAs QDs on both InGaAs and InP[15] and predicted by Yoon et al.[36] Although at the typical droplet temperature of 400 °C the In surface diffusion ρ apparently strongly differs for InGaAs and InGaAsP surfaces, with $\rho_{InGaAs} << \rho_{InGaAsP}$ as discussed above (see also Figure 3 as reference) we observe that, after crystallization, QDs on both layers present a similar density of 1×10^{10} cm^{-2} versus 2×10^{10} cm^{-2} for InGaAs and InGaAsP, respectively (Figure 5c,d). We ascribe this phenomenon to a modification of the surface kinetics triggered by temperature and the As supply during droplet crystallization. Indeed, considering a continuous As supply on the InGaAsP surface during the thermal ramp for crystallization, we expect enhanced As/P exchange reactions at the surface to take place, since the temperature strongly enhances such reactions, following an Arrhenius plot.[37] As a consequence, an As-rich InGaAsP surface is formed during the crystallization step, strongly affecting the In surface diffusion, which becomes comparable to that of InGaAs. This is also in accordance with the LCM model discussed above: under As-overpressure and in the absence of P, the phase separation at the InGaAsP surface will be reduced,[30,31] leading to a surface configuration closer to
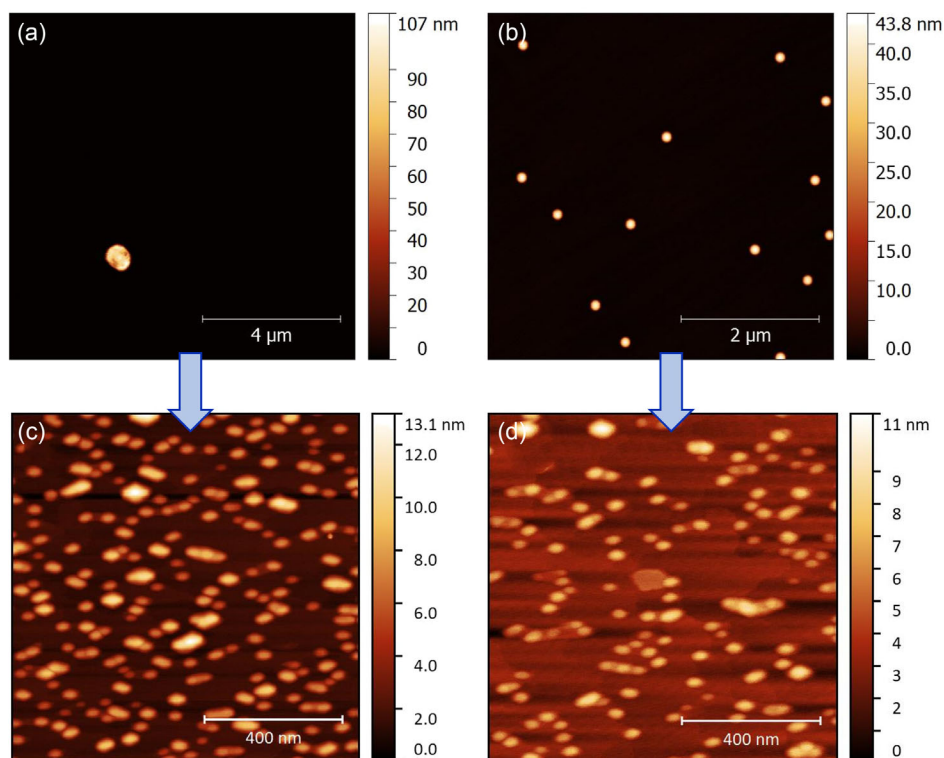
Figure 5. AFM of free-standing Indium droplets and corresponding InAs QDs on a,c) InGaAsP and b,d) InGaAs surfaces.

InGaAs. As a result, this process appears to compensate for the initial difference in In surface diffusion of the metallic indium droplets on the two interlayers. Thus, we observe a similar QD density on both surfaces. Here, we note that the determination of the actual In diffusion parameters for an InGaAsP surface is not accessible by the present growth technique (MOVPE), but would be possible in molecular beam epitaxy (MBE) due to the temperature-dependent size of the "halo" formed around the droplets, which is directly linked to the group-III metallic droplet diffusion length.[29,38–41] In this respect, studies are found for In on InP,[40] In on $In_{0.53}Ga_{0.47}As$,[29] In on $In_{0.52}Al_{0.48}As$,[42] In on GaAs,[41] and Ga on GaAs,[38,39] and to the best of our knowledge, studies of the In diffusion on InGaAsP surfaces are not known. Finally, it is worth pointing out that even though the QDs are not directly formed from the initial droplets as was found for the "standard" DE mode (see, e.g., our previous work on InAs/InP QDs),[12] there is no evidence for the presence of a strained wetting layer, confirmed by the optical characterizations in this work. Additionally, in our previous morphological investigations by XSTM on InAs/InGaAs DE QDs of Figure 5d,[15] we had evidence for the presence of the 5 nm InGaAs interlayer and the QDs nucleated directly on this layer, without the presence of a wetting layer.

To summarize, the overall effect of the As-containing interlayers (both InGaAs and InGaAsP) appears to be threefold: 1) modification of the In adatom diffusion and thus droplet formation (decreased for InGaAs and increased for InGaAsP, compared to InP), 2) modified droplet crystallization process whereby QDs show a much higher density than the original In droplets, and 3) hindering of the formation of long-range etch pits on the

InP surface, and suppression of the formation of a 2D $In_xAs_{1-x}P$ quasi-wetting layer, as previously observed by us for InAs/InGaAs/InP.[14,15]

After discussing the droplet crystallization dynamics, we study the dependence of QD density on varying droplet deposition temperatures on the InGaAsP surface. **Figure 6** shows AFM micrographs of free-standing surface QDs after crystallization, for the five different droplet temperatures considered before. For all temperatures, QDs can be clearly detected, even when previously for temperatures of less than 350 °C no macroscopic droplets were observed. This phenomenon is explained as follows: for a droplet temperature of less than 320 °C, the indium precursor trimethylindium is not pyrolyzed, i.e., broken down into methylindium groups.[26,27] An increase in temperature during the thermal ramp will trigger a gradual decomposition of methylindium occurring at the surface,[43,44] and providing metallic indium available for droplet formation. This is in accordance with the fact that the methylindium molecules not yet pyrolyzed are involatile and remain on the surface until they are fully broken down at ≈480 °C.[26] Subsequently, droplets will be crystallized into QDs by the As supply. For a temperature equal to 320 °C, the In initial wetting of the surface will coalesce into droplets during the ramp, and then become crystallized into QDs. We note that the presence of this indium wetting is also the origin of the rough morphology observed in Figure 1c for this droplet temperature.

The plot in Figure 6f shows the trend of the QD density with increasing droplet deposition temperature, while **Figure 7** shows the variation of QD size. For a droplet temperature of 250 °C, the resulting QDs have a density of 8×10^8 cm^{-2}, a width of (96 ± 16) nm, and a height of (4.7 ± 0.9) nm. With increasing temperature, the QD density rises sharply by of one order of
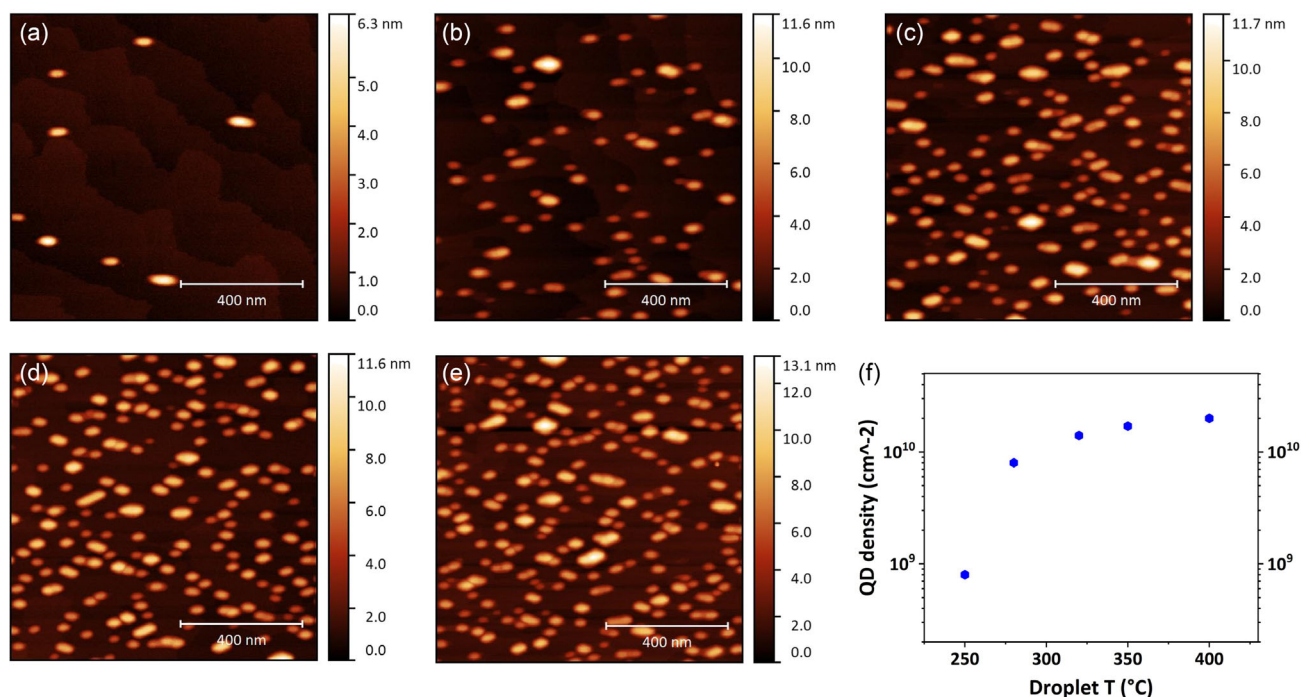
Figure 6. AFM micrographs of free-standing InAs/InGaAsP QDs with variation of droplet deposition temperature: a) 250 °C, b) 280 °C, c) 320 °C, d) 350 °C, and e) 400 °C. In f) QD density versus initial droplet density is displayed.
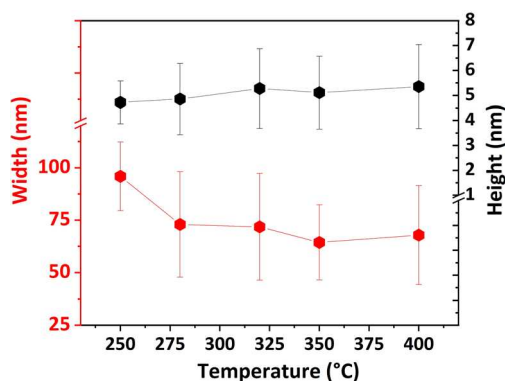
Figure 7. QD widths and heights versus droplet deposition temperature.

magnitude at 280 °C, whereas QDs have an overall reduced width of (73 ± 25) nm and height of (4.8 ± 1.4) nm. At 320 °C, the density exceeds 10^{10} cm^{-2} while the QD widths reduce overall. At 400 °C, the QD size shows a slight increase, with width of (67.8 ± 24) and height of (5.3 ± 1.7) nm and their density reaches $\approx 2 \times 10^{10}$ cm^{-2}. Further increasing the droplet temperature beyond 400 °C leads to surface degradation due to defect formation (enhanced material coalescence).

Finally, we also note that such InAs QDs on InGaAsP do not show dash-like features (QDashes), such as strong elongation toward a preferential crystallographic direction,[45–47] regardless of the droplet temperature used. It is well-known that InAs on InGaAsP layers grown on exact InP(100) surfaces naturally grows as dashes, often showing coexistence of nanostructures with various shapes if the growth conditions are not carefully optimized, both in MBE and MOVPE.[43–45] The formation of dashes for the system InAs/InP is favored by the low lattice mismatch between InP and InAs ($\approx 3\%$) and the low surface energy of (114)A InAs facets.[45] Here, we ascribe the absence of QDashes to the fact that the DE method does not rely on the lattice mismatch between surface and epilayer, thus allowing for a better control of QD formation, which is decoupled from the layer/epilayer mismatch. Thus, by employing DE we can overcome this issue and promote the formation of QDs over QDashes. We note that

this is a property of DE and has a general validity, and it applies also to other surfaces, e.g., InP and InGaAs.[12,14]

To investigate the optical properties of QDs, RT-PL, and LT-µPL characterizations were performed. **Figure 8**a shows RT-PL spectra of samples containing the QDs grown under the same conditions as presented in Figure 6 for morphological analysis (e.g., grown with droplet temperatures of 250–400 °C). All samples show clear PL emission in the range 1400–2200 nm. In the temperature range of 250–320 °C, the QD emission blueshifts by ≈ 100 nm (1870–1770 nm), then between 320 and 350 °C it redshifts by ≈ 60 nm, eventually stabilizing around 1830 nm at 400 °C, see Figure 8b. We ascribe the first blueshift to an increased number of small QDs nucleating in that temperature range, as can also be seen in the AFM micrographs of Figure 6 and in the plot of Figure 7, where especially the QD width decreases. Whilst we observe a slight redshift in the range 320–350 °C, we note that the average widths and heights at 350 °C decrease. This phenomenon could be explained by a greater contribution of electronic states of larger QDs at longer wavelengths, driven by the higher droplet temperature promoting a better crystal quality. The inset of Figure 8a shows the integrated intensity of the PL spectra as a function of droplet temperature. The intensity increases together with the QD density until 350 °C and then decreases abruptly at 400 °C. This reflects the increasing number of emitting QDs contributing to the overall PL until 350 °C. At 350 °C the integrated intensity is the largest, suggesting that the majority of optically active QDs are found for this temperature. The decrease in integrated intensity at 400 °C, together with a stabilization in the emission wavelength and the slight increase in the average size, indicates the possible formation of defects, such as giant QDs, not contributing to the PL emission. However, we note that the samples at temperatures greater than 250 °C show a relatively low radiative efficiency, considering that on average their QD densities are one order of magnitude higher than the sample at 250 °C. This suggests that, overall, the PL efficiency of the higher-density dots is lower. Finally, it is also worth pointing out that no luminescence from the InGaAsP interlayer is detectable in the RT-PL spectra, in contrast to the previous InAs/InGaAs QDs at the same growth conditions (here, we refer the reader to Figure 5 of Ref.[14]), and
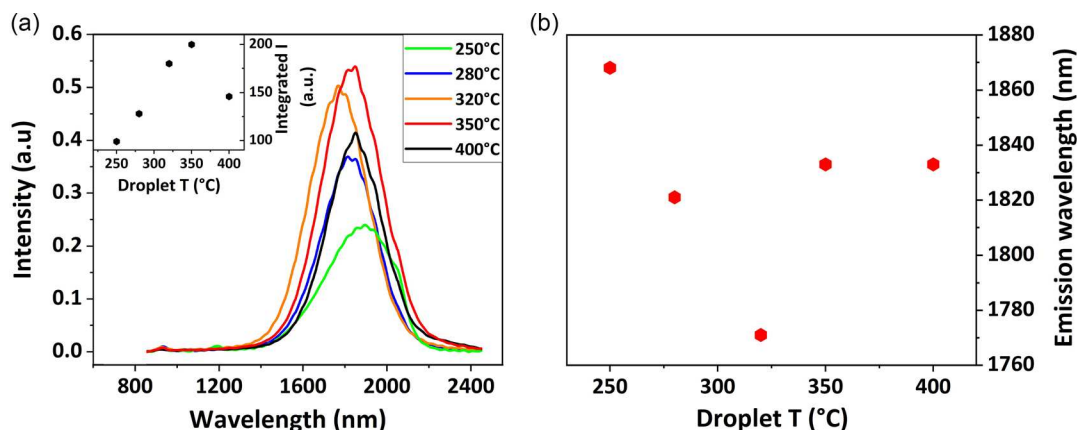

Figure 8. a) RT-PL of QD-ensembles with QDs grown with increasing droplet temperature in the range 250–400 °C. In the inset, the PL integrated intensity versus droplet temperature is shown. b) PL peak emission wavelength versus droplet temperature.

where the emission of the InGaAs interlayer was always present. This points to an overall more efficient carrier capture at RT into QDs grown on an InGaAsP layer instead of InGaAs. This aspect could be of advantage for the use of such QDs in photonic applications. A detailed study on the carrier dynamics and radiative efficiency for InAs QDs on InGaAsP and InGaAs layers goes beyond the scope of the present work, and currently, dedicated optical investigations are underway.

LT-µPL investigations were also carried out, at both high and low power, e.g., with 450 and 4.5 W cm^{-2} excitation respectively. At high power, (**Figure 9**a), one can clearly see a bright emission of the InGaAsP layer at around 1130 nm for a droplet temperature of 250 °C. At droplet temperatures of 280 °C, such emission strongly quenches but remains detectable around the same wavelength, while at higher temperatures it quenches fully.

The QD ensemble emission is detected for all temperatures in the spectral region of 1300–1600 nm (detector cut-off), being the weakest for 250 °C. Low-power µPL of Figure 9b shows the presence of high-density bright single lines as a signature of single-dot emission. No single-dot emission is observed for 250 °C, even though clear QD PL was observed at RT, Figure 8a, and a weak QD ensemble emission at LT (Figure 9a). We ascribe this phenomenon to interface roughness and composition inhomogeneities of the QW which at low temperature efficiently confines carriers and provide localized states showing δ-like luminescence.[48,49] In our samples, these are apparently more efficient in trapping carriers compared to QDs. We expect indeed the InGaAsP QW to provide a high number of these states due to compositional fluctuations and we also refer to the above discussion on the LCM of such QWs. In contrast, at RT the carriers undergo a redistribution to lower energy states due to the
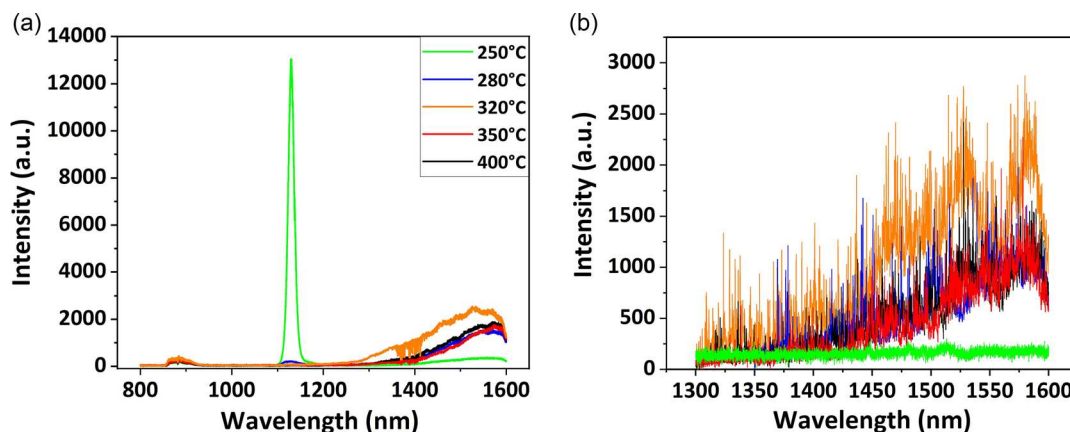
Figure 9. LT-µPL at a) high and b) low power of QD-ensembles grown with increasing droplet temperature in the range 250–400 °C. Same color scale used for both graphs.
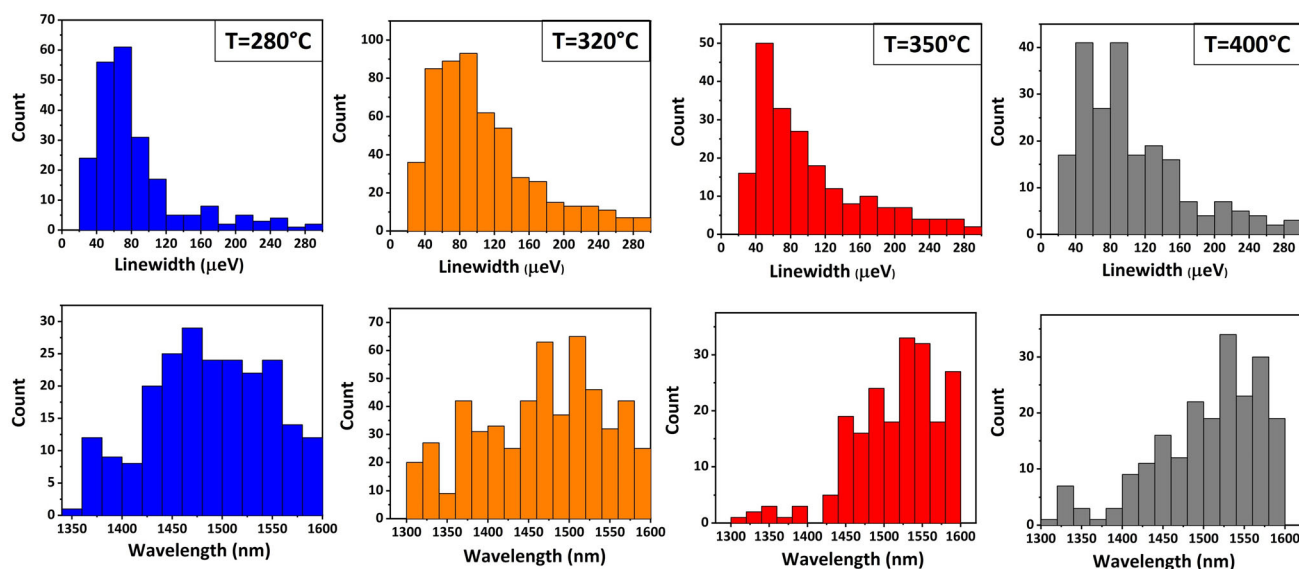
Figure 10. Linewidth and wavelength distributions for single-dot emission for the temperature range of 280–400 °C.

temperature-dependent increase in mobility,[48,49] and they are more likely to recombine in the QDs; hence the luminescence seen in Figure 8a. The absence of any wetting layer emission in all PL spectra confirms the nature of the QD growth studied in this work being DE and not any form of SK growth.

Finally, we analyzed the wavelength and linewidth distributions of single dot emission of QDs in the range 280–400 °C. In **Figure 10**, histograms of such distributions are presented (same color scale used as before). The data were fitted by using log-normal distributions. All QDs cover the technologically relevant C-band, spanning between the O and the L-band. QDs at 280 °C have the sharpest linewidth distribution of (85 ± 53) μeV with associated wavelength distribution of (1486 ± 59) nm. For 320, 350, and 400 °C, linewidths are of (107 ± 89), (101 ± 63), and (105 ± 60) μeV, respectively, and wavelengths of (1464 ± 67), (1515 ± 57), and (1504 ± 66) nm, respectively. We note that most QDs (except those at 280 °C having lower density) show relatively broad linewidths >100 μeV. This could be due to the high QD density resulting in intradot coupling or charge noise in the vicinity of the QDs which leads to fluctuations in the local electric field and thus significantly affecting the linewidths.[50–52]

3. Conclusion

In this work, we have explored for the first time the growth of telecom InAs QDs on an InGaAsP (Q1.3) interlayer lattice matched to InP, by droplet epitaxy in a MOVPE environment. We have also studied the morphology of In droplets at different deposition temperatures and compared their nucleation on InGaAsP with InGaAs and InP surfaces previously investigated by us. Our data show that the In surface diffusion, and thus the droplet formation, is strongly affected by the surface type at droplet deposition temperatures. For an InGaAsP surface, such variation is almost completely compensated by temperature during the crystallization phase, via As/P exchange leading to an As-terminated InGaAsP surface. This has led to a similar QD nucleation process to InGaAs, e.g., a modified droplet epitaxy mechanism. We have thus shown that the insertion of the As-containing interlayers modifies the growth kinetics from a mass-transport observed for bare InP to a surface-reaction limited regime, where the formation of the etching pits and the 2D quasi-wetting layer are suppressed, and the QDs present a much higher density compared to the initial droplets. Optical investigations show QD ensemble emission at RT and bright single-dot emission at LT, the latter covering the technologically relevant telecom C-band, making such QDs suitable for quantum technology applications at this wavelength range. Also, as expected by the DE growth mode, we confirm the absence of a wetting layer typical of the SK growth mechanisms. On a final note, we have also shown that the InAs/InGaAsP QDs investigated here reach densities beyond 10^{10} cm^{-2} pointing to a potential use of such QDs as active the medium in InGaAsP-based lasers around the C-band, considering the extensive use of InGaAsP as waveguide material. Additionally, DE allows for a better control of the QD morphology, hindering the formation of elongated nanostructures such as QDashes. With this work, we

demonstrate further success and flexibility of the droplet epitaxy technique in MOVPE for the fabrication of a variety of efficient optical sources for quantum technology applications at telecom wavelengths.

4. Experimental Section

The samples studied here were all grown in a $3 \times 2''$ Close-Coupled Showerhead (CCS) Aixtron MOVPE reactor, using H$_2$ as a carrier gas, on InP(100) substrates. The growth commences with a ≈300 nm InP buffer grown at a substrate temperature of 600 °C. Thereafter, a 5 nm quaternary In$_{0.719}$Ga$_{0.281}$As$_{0.608}$P$_{0.392}$ interlayer (Q1.3, e.g., $\lambda_g = 1.3$ μm bulk at room temperature) lattice-matched to InP is grown at the same temperature using trimethylindium (TMIn), trimethylgallium (TMGa), arsine (AsH$_3$), and phosphine (PH$_3$), with flows of 32, 7.3, 310, and 7×10^3 μmol min^{-1}, respectively. After the growth of this layer, the temperature is decreased to 250–400 °C, depending on the sample, for In droplet deposition. Indium droplets are deposited with a TMIn flow of 20 sccm for 35 s. Next, the temperature is increased to 520 °C under an AsH$_3$ flow of 24 μmol min^{-1} for complete droplet crystallization into InAs QDs. Thereafter, QDs are capped at the same temperature of 520 °C with ≈20 nm InP to bury them and the structure is completed with a further ≈80 nm InP layer growth at 600 °C for optical characterizations. For morphological characterizations via atomic force microscopy (AFM), the QDs are instead left uncapped, thus free-standing. To allow for a better evaluation of the droplet density over larger areas compared to AFM, scanning electron microscopy (SEM) investigations were carried out on droplet-only samples, with an acceleration voltage of 10 kV and magnifications of 5000 and 30 000. Finally, for room-temperature photoluminescence (RT-PL) characterization, the samples were excited with a 645 nm diode laser having 85 W cm^{-2} power density. For low-temperature micro-PL (LT-μPL), samples were cooled down to 4 K and excited with a 635 nm laser with a power density of 4.5 and 450 W cm^{-2} for low and high power, respectively, and with a spectrometer resolution of 25 μeV. LT-μPL measurements were carried out on ensembles of QDs, with a collection spot size of ≈5 μm diameter.

Conflict of Interest

The authors declare no conflict of interest.

Author Contributions

E.M.S. and J.H. conceived the idea for this work. Y.I.N. performed SEM, AFM, and μPL investigations. M.G. also performed μPL and provided assistance with the measurements and related data analysis. E.M.S. designed and grew the samples by MOVPE and performed RT-PL. E.M.S. and Y.I.N. analyzed the data. E.M.S. wrote the manuscript and all authors contributed to its editing. J.H. provided overall supervision. All authors have approved the final version of the manuscript.

**ADVANCED
SCIENCE NEWS**

www.advancedsciencenews.com

pssrrl

physica status solidi

www.pss-rapid.com

Data Availability Statement

Keywords

[1] D. Bimberg, M. Grundmann, N. N. Ledentsov, *Quantum Dot Heterostructures*, Wiley, Chichester **1999**.

[2] V. A. Shchukin, N. N. Ledentsov, D. Bimberg, *Epitaxy of Nanostructures*, Springer, Berlin/New York **2003**.

[3] N. N. Ledentsov, *Semicond. Sci. Technol.* **2011**, *26*, 014001.

[4] D. Bimberg, *Electron. Lett.* **2008**, *40*, 168.

[5] D. Bimberg, M. Grundmann, F. Heinrichsdorff, N. N. Ledentsov, V. M. Ustinov, A. E. Zhukov, A. R. Kovsh, M. V. Maximov, Y. M. Shernyakov, B. V. Volovik, A. F. Tsatsul'nikov, P. S. Kop'ev, Z. I. Alferov, *Thin Solid Films* **2000**, *367*, 235.

[6] P. Michler, *Quantum Dots for Quantum Information Technologies*, Springer, Berlin/New York **2017**.

[7] A. Marent, T. Nowozin, M. Geller, D. Bimberg, *Semicond. Sci. Technol.* **2011**, *26*, 014026.

[8] E. M. Sala, I. F. Arikan, L. Bonato, F. Bertram, P. Veit, J. Christen, A. Strittmatter, D. Bimberg, *Phys. Status Solidi B* **2018**, *255*, 1800182.

[9] L. Bonato, E. M. Sala, G. Stracke, T. Nowozin, A. Strittmatter, M. N. Ajour, K. Daqrouq, D. Bimberg, *Appl. Phys. Lett.* **2015**, *106*, 042102.

[10] T. Müller, J. Skiba-Szymanska, A. B. Krysa, J. Huwer, M. Felle, M. Anderson, R. M. Stevenson, J. Heffernan, D. A. Ritchie, A. J. Shields, *Nat. Comm.* **2018**, *9*, 862.

[11] P. Holewa, M. Gawełczyk, C. Ciostek, P. Wyborski, S. Kadkhodazadeh, E. Semenova, M. Syperek, *Phys. Rev. B* **2020**, *101*, 195304.

[12] E. M. Sala, Y. I. Na, M. Godsland, A. Trapalis, J. Heffernan, *Phys. Status Solidi RRL* **2020**, *14*, 2000173.

[13] E. M. Sala, M. Godsland, A. Trapalis, J. Heffernan, *Phys. Status Solidi RRL* **2021**, *15*, 2100283.

[14] E. M. Sala, M. Godsland, Y. I. Na, A. Trapalis, J. Heffernan, *Nanotechnology* **2022**, *33*, 065601.

[15] R. S. R. Gajjela, E. M. Sala, J. Heffernan, P. M. Koenraad, *ACS Appl. Nano Mater.* **2022**, *5*, 8070.

[16] N. Ha, T. Mano, T. Kuroda, K. Mitsuishi, A. Ohtake, A. Castellano, S. Sanguinetti, T. Noda, Y. Sakuma, K. Sakoda, *Jpn. J. Appl. Phys.* **2015**, *54*, 04DH07.

[17] A. Tuktamyshev, A. Fedorov, S. Bietti, S. Vichi, K. D. Zeuner, K. D. Jöns, D. Chrastina, S. Tsukamoto, V. Zwiller, M. Gurioli, S. Sanguinetti, *Appl. Phys. Lett.* **2021**, *118*, 133102.

[18] M. Paul, F. Olbrich, J. Höschele, S. Schreirer, J. Kettler, S. L. Portalupi, M. Jetter, P. Michler, *Appl. Phys. Lett.* **2017**, *111*, 033102.

[19] J. Skiba-Szymanska, R. M. Stevenson, C. Varnava, M. Felle, J. Huwer, T. Müller, A. J. Bennett, J. P. Lee, I. Farrer, A. B. Krysa, P. Spencer, L. E. Goff, D. A. Ritchie, J. Heffernan, A. J. Shields, *Phys. Rev. Appl.* **2017**, *8*, 014013.

[20] M. Anderson, T. Müller, J. Skiba-Szymanska, A. B. Krysa, J. Huwer, R. M. Stevenson, D. A. Ritchie, A. J. Shields, *Appl. Phys. Lett.* **2021**, *118*, 014003.

[21] M. Gurioli, Z. Wang, A. Rastelli, T. Kuroda, S. Sanguinetti, *Nat. Mater.* **2019**, *18*, 799.

[22] M. Razeghi, *Nature* **1994**, *369*, 631.

[23] T. Sadeev, D. Arsenijević, D. Bimberg, *Appl. Phys. Lett.* **2016**, *109*, 161104.

[24] S. Anantathanasarn, R. Nötzel, P. J. Van Veldhoven, T. J. Eijkemans, J. H. Wolter, *Appl. Phys. Lett.* **2006**, *89*, 073115.

[25] V. Thévenot, V. Souliere, H. Dumont, Y. Monteil, J. Bouix, P. Regreny, T.-M. Duc, *J. Cryst. Growth* **1997**, *170*, 251.

[26] M. G. Jacko, S. J. W. Price, *Can J. Chem.* **1964**, *42*, 1198.

[27] N. I. Buchan, C. A. Larsen, G. B. Stringfellow, *J. Cryst. Growth* **1988**, *92*, 591.

[28] C. Park, W.-S. Jung, Z. Huang, T. J. Anderson, *J. Mater. Chem.* **2002**, *12*, 356.

[29] M. A. Stevens, S. Tomasulo, S. Maximenko, T. E. Vandervelde, M. K. Yakes, *J. Appl. Phys.* **2017**, *121*, 19.

[30] R. R. LaPierre, B. J. Robinson, D. A. Thompson, *Appl. Surf. Sci.* **1995**, *90*, 437.

[31] R. R. LaPierre, T. Okada, B. J. Robinson, D. A. Thompson, G. C. Weatherly, *J. Cryst. Growth* **1996**, *158*, 6.

[32] C. K. W. Wyllie, D. A. Thompson, *Semicond. Sci. Technol.* **1998**, *13*, 750.

[33] T. L. McDevitt, S. Mahajan, D. E. Laughlin, W. A. Bonner, V. G. Keramidas, *Phys. Rev. B* **1992**, *45*, 12.

[34] R. R. LaPierre, B. J. Robinson, D. A. Thompson, *J. Cryst. Growth* **1998**, *191*, 319.

[35] R. K. Akchurin, I. A. Boginskaya, N. T. Vagapova, A. A. Marmalyuk, M. A. Ladugin, *Tech. Phys. Lett.* **2010**, *36*, 724.

[36] S. Yoon, Y. Moon, T. W. Lee, H. Hwang, E. Yoon, Y. D. Kim, *Thin Solid Films* **1999**, *357*, 81.

[37] N. Kobayashi, Y. Kobayashi, *J. Cryst. Growth* **1992**, *124*, 525.

[38] J. S. Kim, *Mater. Sci. Semicond. Process.* **2017**, *57*, 70.

[39] S. Bietti, C. Somaschini, L. Esposito, A. Fedorov, S. Sanguinetti, *J. Appl. Phys.* **2014**, *116*, 114311.

[40] D. Fuster, K. Abderrafi, B. Alen, Y. Gonzalez, L. Wewior, L. Gonzalez, *J. Cryst. Growth* **2016**, *434*, 81.

[41] T. Noda, T. Mano, H. Sakaki, *Cryst. Growth Des.* **2011**, *11*, 726.

[42] M. A. Stevens, W. McKenzie, G. Baumgartner, J. Q. Grim, S. G. Carter, A. S. Bracker, *J. Vac. Sci. Technol. A* **2023**, *41*, 032703.

[43] J. Haigh, S. O'Brien, *J. Cryst. Growth* **1984**, *67*, 75.

[44] J. Haigh, S. O'Brien, *J. Cryst. Growth* **1984**, *68*, 550.

[45] A. Ponchet, L. Pedesseau, A. Le Corre, C. Cornet, N. Bertru, *Appl. Phys. Lett.* **2019**, *114*, 173102.

[46] N. Sritirawisarn, F. W. M. Van Otten, T. J. Eijkemans, R. Nötzel, *J. Cryst. Growth* **2007**, *305*, 63.

[47] A. Lenz, F. Genz, H. Eisele, L. Ivanova, R. Timm, D. Franke, H. Künzel, U. W. Pohl, M. Dähne, *Appl. Phys. Lett.* **2009**, *95*, 203105.

[48] A. Polimeni, A. Patane', M. Henini, L. Eaves, P. C. Main, *Phys. Rev. B* **1999**, *7*, 59.

[49] R. Zimmermann, E. Runge, *Phys. Stat. Sol. A* **1997**, *164*, 511.

[50] A. Högele, S. Seidl, M. Kroner, K. Karrai, R. J. Warburton, B. D. Gerardot, P. M. Petroff, *Phys. Rev. Lett.* **2004**, *93*, 217401.

[51] M. Atatüre, J. Dreiser, A. Badolato, A. Högele, K. Karrai, A. Imamoglu, *Science* **2006**, *312*, 551.

[52] J. Houel, A. V. Kuhlmann, L. Greuter, F. Xue, M. Poggio, B. D. Gerardot, P. A. Dalgarno, A. Badolato, P. M. Petroff, A. Ludwig, D. Reuter, A. D. Wieck, R. Warburton, *Phys. Rev. Lett.* **2012**, *108*, 107401.